# Effects of Macromolecular Crowding on Amyloid Beta (16−22) Aggregation Using Coarse-Grained Simulations

David C. Latshaw,[‡] Mookyung Cheon,[†] and Carol K. Hall*[,‡]

[†]Center for Proteome Biophysics, Department of New Biology, Daegu Gyeongbuk Institute of Science and Technology (DGIST), Daegu 711-873, Korea

[‡]Department of Chemical and Biomolecular Engineering, North Carolina State University, Raleigh, North Carolina 27695-7905, United States

ABSTRACT: To examine the effect of crowding on protein aggregation, discontinuous molecular dynamics (DMD) simulations combined with an intermediate resolution protein model, PRIME20, were applied to a peptide/crowder system. The systems contained 192 Aβ(16−22) peptides and crowders of diameters 5, 20, and 40 Å, represented here by simple hard spheres, at crowder volume fractions of 0.00, 0.10, and 0.20. Results show that both crowder volume fraction and crowder diameter have a large impact on fibril and oligomer formation. The addition of crowders to a system of peptides increases the rate of oligomer formation, shifting from a slow ordered formation of oligomers in the absence of crowders, similar to nucleated polymerization, to a fast collapse of peptides and subsequent rearrangement characteristic of nucleated conformational conversion with a high maximum in the number of peptides in oligomers as the total crowder surface area increases. The rate of conversion from oligomers to fibrils also increases with increasing total crowder surface area, giving rise to an increased rate of fibril growth. In all cases, larger volume fractions and smaller crowders provide the greatest aggregation enhancement effects. We also show that the size of the crowders influences the formation of specific oligomer sizes. In our simulations, the 40 Å crowders enhance the number of dimers relative to the numbers of trimers, hexamers, pentamers, and hexamers, while the 5 Å crowders enhance the number of hexamers relative to the numbers of dimers, trimers, tetramers, and pentamers. These results are in qualitative agreement with previous experimental and theoretical work.
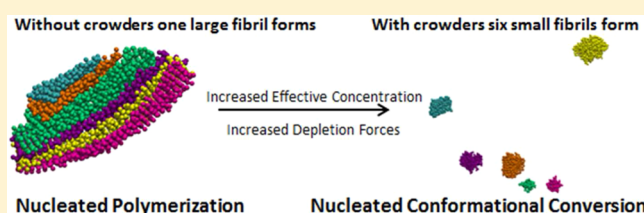
■ INTRODUCTION

Amyloid fibrils are found in over 40 human disorders including Alzheimer's, Parkinson's, and the prion diseases.[1] Each disorder is associated with the aggregation of a distinct protein. In Alzheimer's disease (AD), it is the amyloid β (Aβ) peptide that aggregates to form oligomers (structures consisting of multiple monomeric Aβ subunits) and eventually fibrils and plaques. Although the fibrils and plaques that are found in the brains of AD patients were once thought to be the cause of AD, more recently attention has shifted to the oligomers as the toxic agent, one reason being that small concentrations of prefibrillar oligomers can cause neuronal cell death in the absence of fibrils.[2] This new view of AD etiology has catalyzed investigations of the peptide assembly pathway leading from monomers to oligomers to fibrils, the hope being that this could reveal which parts of the aggregation pathway might serve as potential targets for drugs aimed at treating AD. Most of these studies are done in vitro, since this is the most straightforward way to probe the biophysics underlying the assembly process. In vitro investigations do not, however, capture the influence of biomolecules on Aβ assembly that would occur in vivo.[3,4] In fact, the rate and extent of oligomer/fibril formation in a crowded environment like the human brain can differ by orders of magnitude from that in vitro.[5] The intracellular and extracellular environments in the human brain

are quite crowded with approximately 7% to >40% of the total volume occupied by a variety of macromolecules and structures.[6−8] In this paper, we use computer simulations to learn how crowding affects fibril and oligomer formation as well as aggregation mechanisms.

The influence of crowding agents on the aggregation of proteins has been the subject of a number of experimentally based investigations. Hatters et al. examined the effects of adding dextran 10 at dextran volume fractions of up to $\phi = 0.11$ on the fibrillization of apolipoprotein C-II (apoC-II).[9] Despite the fact that a significant portion of the solution was occupied by dextran 10, the protein's fibril structure was unchanged compared to that in the absence of crowding. Another important finding was that dextran 10 did not interact directly with apoC-II, indicating that it was simply the volume excluded by dextran 10 that accelerated apoC-II fibrillization, not a crowder−peptide interaction. Uversky et al. did a comprehensive investigation of how different crowding agents influence the fibrillization of α-synuclein.[10] Polyethylene glycol (PEG), dextran, ficoll, lysozyme, and bovine serum albumin (BSA) all decreased fibrillization lag time and increased the rate of

fibrillization, but the effects were more pronounced with some crowders than with others. At constant concentration, crowders with longer chain lengths promoted aggregation faster than those with shorter chain lengths. Munishkina et al. explored the effect of macromolecular crowding on the aggregation pathways of four different proteins: a disordered form of S-carboxymethyl-α-lactalbumin, the natively disordered α-synuclein, bovine core histone, and the folded monomeric and hexameric forms of human insulin. They found that, if the protein preferentially adopts a multimeric native state (the bovine histone core and hexameric human insulin both occur naturally in a multimeric state), the fibrillization of that protein is slowed because the multimeric species is stabilized by the crowders. They also found that the fibrillization of proteins that have a low degree of native structure is accelerated by crowding. They interpreted their results to mean that crowding may accelerate fibrillization because it can promote the formation of a partially folded form of the protein that is highly amyloidogenic. Fung et al. examined the effect of adding the simple saccharides glucose, galactose, fructose, mannose, and sucrose on the aggregation of Aβ40 and Aβ42.[11] They found that the sugars that do not directly interact with Aβ promote fibril formation, while the sugars that do interact with Aβ (in their case through hydrogen bonding) promote nucleation and the formation of smaller protofibrils. In a similar vein, Sukenik et al. examined the effects of polyol osmolytes, glycerol and sorbitol, and PEG on the aggregation of a synthetic peptide, MET16, that folds into a β-hairpin and can aggregate into a fibrillar structure.[12,13] Variations in the molecular weight of PEG, glycerol, and sorbitol produced minimal variation in the fibrillization rate, but the polyol osmolytes increased the lag time for fibril formation and increased the fibrillar mass at equilibrium. The authors suggested that the strong polyol osmolyte effect was due to its distortion of the water hydrogen bond network which could change the preferred conformation of the peptides, altering their preferred aggregation state. Upon fitting circular dichroism and ThT fluorescence aggregation data to a simple kinetic model, they discovered that addition of PEG leads to extensive fibril fragmentation, while addition of polyol osmolytes stabilized fibrillar structures by decreasing monomer dissociation.

The impact of crowding on protein aggregation has also been investigated using theory. The Minton group has shown that macromolecular crowding has different effects on protein aggregation, depending on what the rate limiting aggregation mechanism is.[14,15] Aggregation that is slow and reaction-limited is typically enhanced by the presence of crowders because the crowders increase the effective protein concentration and create depletion forces between the proteins, while fast, diffusion-limited aggregation is hindered by crowders because diffusion decreases with increasing crowder concentration.[16] For example, since the dock-lock mechanism that is believed to govern Aβ fibrillization is essentially a reaction-limited process, the presence of crowders should increase fibrillization.[17] In a series of papers by Kinjo and Takada, the effects of macromolecular crowding and chaperones on protein aggregation and folding were examined using density functional theory in conjunction with dynamic rate equations.[18−20] Aggregation, folded−unfolded protein reactions, and protein−chaperone binding reactions were modeled by diffusion and the dynamic rate equations. Proteins, crowders, and chaperones were modeled using hard spheres with square well potentials. They found that crowding enhanced the aggregation of the model

unfolded proteins but stabilized the model native state proteins as long as they were uniformly distributed in space. They also found that crowding accelerated the transition from unfolded to folded model protein if the folding rate was fast, and destabilized model proteins if the folding rate was slow, which is in agreement with Zhou et al.[16] More recently, Minton examined theoretical models that incorporated a time-dependent macromolecular crowder concentration to mirror the observation that the concentration of soluble proteins in the human brain tends to increase linearly with time.[21] The major conclusion of this study was that rate constants for protein aggregation are undetectably small in the absence of crowders, and that the accumulation of crowders over time is what increases the rate constants to a level that actually induces aggregation. As the crowder concentration increased linearly with time, the aggregation rate constant also increased, at a minimum, exponentially.

Molecular-level simulations have also been used to examine the effect of crowding on protein aggregation. O'Brien et al. conducted atomistic simulations in implicit solvent to examine how crowder volume fraction, size, and shape affected the oligomerization of a 10-residue fragment of the transthyretin (TTR) protein.[22] The crowders were modeled as softly repulsive spheres of diameter 7, 12, and 22 Å and as spherocylinders with diameter 7 Å and length 23.1 Å; the simulations were performed on a system containing two to four peptides at a concentration of 15−31 mM with crowder volume fractions of ϕ = 0.05−0.20. They observed that adding crowders of any size and concentration to the simulation enhanced aggregation. One interesting result was that the addition of spherical crowders to the simulations destabilized TTR dimers in favor of trimeric and tetrameric oligomers. They also found that, as the size of the crowding spheres increased, the level of aggregation enhancement decreased. Finally, sphereocylinder crowders destabilized the oligomers to a larger extent than the spherical crowders, highlighting the importance of the shape of crowding molecules. Magno et al. simulated a system of 125 amphipathic 10-bead coarse-grained polypeptides designed specifically for studying the physics of fibril formation; i.e., the model peptide did not represent a specific sequence or have a defined length.[23] The peptide had a tunable energy parameter that could be shifted from an aggregation-prone state (β-state, which favors a cross-β structure) to an aggregation-protected state (π-state, which favors a monomeric state). Their general conclusion was that crowding greatly accelerates the aggregation of peptides that have a reaction-limited aggregation mechanism but only modestly accelerates the aggregation of peptides that have a diffusion-limited aggregation mechanism. The former conclusion agrees with that of Ellis and Minton, but the latter conclusion does not.[14] The Magno et al. polypeptide model is well suited for a fundamental study of protein aggregation in the presence of crowders, but it does not provide any information about the effects of crowding on more complex proteins. Co et al. used lattice Monte Carlo to simulate the effects of crowding and confinement on the fibrillization of 6, 10, and 24 peptides using a toy model with the sequence +HHPPHH−, where + is positive, − is negative, H is hydrophobic, and P is polar.[24] The sequence was designed to fold into a compact U-shape similar to a β-hairpin. Crowders were modeled as squares or rectangles on the lattice, and confinement was modeled using a box with hard walls. They showed that crowding and confinement can decrease fibrillization lag time up to intermediate values of

crowder surface area and confinement box length, after which the lag time begins to increase. Their results highlighted the complex nature of crowding, with longer fibrillization lag times at both high and low crowder concentrations, as predicted by Zimmerman and Minton,[8] and recently observed by Cabaleiro-Lago et al. using amine-modified polystyrene nanoparticles.[25]

The physical picture that emerges concerning the effects of crowders on protein aggregation is reminiscent of that concerning the effects of crowders on protein folding. Zhou et al. summarize the effects of crowding on protein folding in terms of the existence of an energy barrier to folding that is a function of the amount of space that a protein must occupy in order to fold.[16] If the folding pathway contains an intermediate that occupies more space than the initially unfolded protein, then the rate of folding will be slowed because crowding prevents the protein from expanding; this raises the energy barrier to folding. If the folding pathway takes the protein through an intermediate that is more compact than the unfolded protein, then the rate of folding tends to be enhanced by crowding because crowding forces the protein into a more collapsed conformation, effectively lowering the folding energy barrier. Additionally, intrachain diffusion in large proteins can be decreased by the presence of crowders, slowing down the overall rate of folding if multiple regions must fold independently before the final tertiary structure is achieved.

These ideas can be generalized to the case of protein oligomerization and fibrillization. While proteins in dilute solution can form a wide variety of aggregate structures through many kinetic pathways, crowded systems have energetic penalties associated with forming aggregates that are not highly compact so the number of kinetic pathways tends to be smaller.[26] In the case of amyloidogenic proteins, a given number of monomers typically occupies more space than an oligomer or fibril made up of the same number of proteins, making monomers less energetically favorable. Additionally, intrinsically disordered proteins which do not have a defined quaternary structure in dilute solution might be driven to interact with each other to form oligomers or fibrils in a crowded environment because they would then occupy less space. The same idea applies to a partially folded protein. A partially folded protein may preferentially interact with other partially folded proteins in the presence of crowders because an aggregate of partially folded proteins is more thermodynamically stable than a bunch of isolated partially folded proteins.

In this paper, we apply a combination of discontinuous molecular dynamics (DMD) and the PRIME20 force field to examine how the aggregation of a multipeptide system containing $A\beta(16-22)$ is impacted by macromolecular crowding. Although $A\beta$ is typically observed in its 40 or 42 residue form, our simulations focus on the $A\beta(16-22)$ peptide, which has been shown to be a key sequence in the formation of $A\beta$ oligomers and fibrils, and has the ability to form fibrils on its own.[27−29] In our simulations, we monitor the aggregation, oligomerization, and fibril formation of a system containing 192 peptides using hard sphere crowders at crowding volume fractions of $\phi = 0.00$, 0.10, and 0.20 and crowder diameters of $D = 5$, 20, and 40 Å. Since oligomeric structures have become important in the study of $A\beta$ toxicity, we also look closely at how crowding affects the stability of oligomers and their conversion to other larger species. We explore how crowding affects peptide association rates, and aggregation mechanisms. We compare our results to theoretical predictions of the effects of crowding on protein aggregation by O'Brien et al.,

Munishkina et al., Zhou et al., and Zimmerman and Minton[8,22,26,30] and provide molecular level detail about how oligomer and fibril formation in a crowded medium differs from that in a dilute solution.

Our simulation results show that when crowders are added to a system of peptides they increase the rate of oligomer formation and the maximum number of oligomers that form. Oligomer formation shifts from being a slow process characterized by the templated addition of monomers to existing oligomers in the absence of crowders to a fast collapse and subsequent rearrangement that leads to a high maximum in the number of oligomers formed when crowders are present. Addition of crowders also increases the rate of conversion from oligomers to fibrils, giving rise to an increased rate of fibril growth. In all cases, larger crowder volume fractions and smaller crowder diameters provide the greatest enhancement of oligomerization and fibrillization. This enhancement is largely a consequence of the depletion forces between the peptides due to the crowders. These forces drive peptide−peptide association, making oligomers and fibrils more thermodynamically favorable than an equivalent number of monomers. Additionally, we have shown that, depending on the size of the crowders relative to the peptides, specific oligomer sizes can be stabilized. In our simulations with 40 Å crowders, the dimers were stabilized and persisted longer relative to the trimers, tetramers, pentamers, and hexamers. We surmise that this is because the 40 Å crowders have interstitial spaces that are large enough to easily accommodate dimers and therefore stabilize them. In contrast, in our simulations with 5 Å crowders, the hexamers are preferentially formed compared to dimers, trimers, tetramers, and pentamers. We believe that, with 5 Å crowders, the formation of these larger oligomeric species is energetically favorable because oligomers allow peptides to take on a conformation that occupies less space than an equivalent number of isolated monomers. Since the oligomer occupies less space, a smaller number of crowders need to be displaced to make room for the structure, making it favorable.

■ METHODS

Discontinuous Molecular Dynamics. The simulation method used in this work is discontinuous molecular dynamics (DMD), a fast alternative to traditional molecular dynamics.[31] In DMD, the potential is a discontinuous function of the interatomic separation, e.g., hard sphere and square well potentials, and since the atoms move linearly between collisions, the only time that the velocities and positions need to be recalculated is when a discontinuity in the potential is encountered. Therefore, the simulation can be advanced from collision event to collision event. The types of discontinuous events in our simulations include hard sphere events, bond events, and square-well and square-shoulder capture and dissociation events.

PRIME20 Force Field. Coarse graining peptide geometry by combining groups of atoms into "united atoms" and then representing them as spheres is an additional way to alleviate the time scale limitations of atomistic MD. One popular coarse-grained model used for studying peptides is a four-sphere-per-residue model in which each amino acid residue is represented by three backbone spheres, one each for N—H, C—H, and C=O and one side-chain sphere R.[32] The four-sphere per residue model provides a balance between accuracy and simplicity that is ideal for DMD. In 2004, our group introduced a new four-sphere-per-residue protein model called PRIME

(protein intermediate resolution model), which was appropriate for homoproteins like polyalanine and polyglutamine.[33−35] In PRIME, all backbone bond lengths and bond angles are fixed at their ideal values, the distance between consecutive Cα atoms is fixed so as to maintain the interpeptide bond in the trans configuration, and the side chains are held in positions relative to the backbone so that all residues are L-isomers.

More recently, PRIME was extended to heteroproteins culminating in PRIME20 which describes the geometry and energetics for all 20 amino acids.[36] The interactions in PRIME20 simulations include excluded volume, hydrogen bonds, hydrophobic interactions, and charge interactions. PRIME20 also includes polar interactions, but Aβ(16−22) does not have any polar amino acids. The parameters used in PRIME20 were derived utilizing a perceptron learning algorithm and a modified stochastic learning algorithm that compared the energy of native state proteins in the Protein Database (PDB) with those of a large number of decoy structures. The parameters used for the Aβ(16−22) peptide in this work are taken from Cheon et al.[37]

Crowder Model. The crowders used in these simulations are modeled as hard spheres of diameter 5, 20, and 40 Å. Thus, the crowder−peptide and crowder−crowder interactions are limited to excluded volume. The 20 Å crowder diameter was selected because it is close to the N- to C-terminal length of a fully extended Aβ(16−22) peptide based on PRIME20 parameters. The 5 and 40 Å crowder diameters were selected to provide contrast for the effects of crowder size on aggregation. The 5 Å crowders are small compared to Aβ(16−22) so they have the ability to sit close to the peptide backbone and in between the side chains, while the 40 Å crowders are significantly larger than Aβ(16−22) and have larger interstitial spaces for the peptides to occupy. In these simulations, the crowder volume fractions examined are ϕ = 0.00, 0.10, and 0.20; the crowder volume fraction is defined as $\phi = NV_0/L^3$, where N is the number of crowders, V_0 is the volume of a single crowder, and L is the simulation box length. These crowder volume fractions correspond to system densities of ρ = 4, 177, and 350 mg/mL, respectively. The system density of 350 mg/mL was chosen as a realistic reference for this work because it is the midpoint between the estimated densities of 300 and 400 mg/mL in cytoplasm and is commonly used as the density for crowding experiments. In order to calculate the internal density of a single crowder molecule necessary to achieve a total system density of 350 mg/mL, we selected a system with a crowder volume fraction of ϕ = 0.20 and crowder diameter of 40 Å as our reference because this seemed closest to physiologically relevant conditions. To make this system have a density of 350 mg/mL, the internal density of a single 40 Å crowder was set at 1.04 Da/Å³. It follows then that the mass of the 40 Å crowder is 34.9 kDa, while the masses of the 20 and 5 Å crowders are 4.4 kDa and 68 Da, respectively. These system parameters were selected on the basis of the recommendations of Ellis and Minton and Zimmerman and Trach for studying macromolecular crowding without exceeding our current computational limitations.[7,14]

Simulation Procedure. Our simulations proceed in the following way: Each simulation contains 192 Aβ(16−22) peptides initially placed at random locations in a cubic simulation box with side lengths of L = 400 Å, giving a peptide concentration of 5 mM, and periodic boundary conditions. The crowders are then placed at random locations surrounding the peptides until the desired crowder volume

fraction is achieved. The reduced temperature is defined as T^* = kT/ε_{HB}, where ε_{HB} is the hydrogen bonding well depth. Velocities for each peptide bead and crowder are chosen at random from a Maxwell−Boltzmann distribution that is centered at the desired temperature. Initially, the temperature is set to T^* = 0.50, a temperature high enough to denature the peptides so as to give them a random coil secondary structure. The system is then gradually cooled stepwise to T^* = 0.193 using a cooling scheme that lasts a total of 14 billion collisions. The reduced temperature T^* = 0.193 was chosen because it is the transition temperature above which fibrillization does not occur for Aβ(16−22). The simulations were performed in the canonical ensemble where the number of particles, temperature, and volume are fixed. The temperature is held constant using the Andersen thermostat method. Beads in the simulation experience random "ghost collisions" with "ghost particles" during which their velocity is reassigned to a random value from a Maxwell−Boltzmann distribution centered at the desired simulation temperature. Up to 15 independent simulations were run for each set of conditions until the number of peptides in oligomers had decayed to $1/e$, or 36.7%, of its maximum value. This amounts to ∼45 billion collisions for the most crowded simulations because aggregation happens more rapidly, and ∼165 billion collisions in the absence of crowders. In our simulations, a peptide is defined as being part of an oligomer if it shares at least one hydrogen bond or one hydrophobic contact with another peptide in the oligomer. A peptide is defined as being part of a β-sheet if it shares at least four hydrogen bonds with another peptide in the β-sheet. A peptide is defined as being part of a fibril if it is in a β-sheet that shares at least four side chain interactions with another β-sheet in the fibril.

Oligomerization Curve Fit and Parameters. Due to the transient nature of oligomers and the small number of peptides that are in an oligomer at any one time, oligomerization data sets can have large variations. To make the trends easier to see, we have fit our data for the number of peptides in oligomers vs reduced time with an asymmetric double sigmoidal function.[38] Reduced time is defined as $t^* = t/\sigma(k_b T/m)^{1/2}$, where σ and m are the average bead diameter and average mass. The asymmetric double sigmoidal function is typically used to fit chromatography data because it can account for a sudden increase followed by a gradual decrease in a data set. We chose it because it nicely fits all our oligomerization data sets; to our knowledge, there is no well-established equation for fitting oligomerization data sets vs time. The asymmetric double sigmoidal function is expressed in eq 1

$$N_{olig}(t^*) = N_0 + A\left(\frac{1}{1 + \exp((t^* - t_{center} + w_1/2)/w_2)}\right)$$
$$\times \left(1 - \frac{1}{1 + \exp((t^* - t_{center} - w_1/2)/w_3)}\right)$$

(1)

where $N_{olig}(t^*)$ is the number of peptides in an oligomer at time t^*, N_0 is the initial number of peptides in an oligomer, A is the amplitude, t_{center} is the center of the peak, and w_1, w_2, and w_3 are widths for the sigmoidal curves. Using this curve fit makes it straightforward to calculate the oligomer growth rate, the maximum number of peptides in oligomers, and the rate of conversion from oligomers to fibrils. To calculate the oligomer growth rate, we find the most linear portion of the curve

between $t* = 0$ and the time at which the number of peptides in oligomers reaches its maximum, t_{peak}, by calculating the R^2 value. We then calculate the slope using the most linear portion of the curve. The maximum number of peptides in oligomers is taken as the maximum in the asymmetric double sigmoidal function, and the oligomer to fibril conversion time is calculated as the amount of time it takes for the number of oligomers to decay from its maximum value to $1/e$, or 36.7%, of its peak value. The average R^2 value for our curve fitting of the number of peptides in oligomers vs reduced time with the asymmetric double sigmoidal function was 0.92. The average R^2 value for our curve fitting of the number of peptides in dimers, trimers, tetramers, pentamers, and hexamers vs reduced time with the asymmetric double sigmoidal function was 0.83.

Small Oligomer Free Energy Analysis. To understand if dimers, trimers, tetramers, pentamers, or hexamers are energetically favorable in the presence of crowders, we analyze the change in free energy associated with forming small oligomers from monomers using a method introduced by Obrien et al.[22] Using the Asakura and Oosawa theory for two bodies immersed in a solution of macromolecules along with scaled particle theory, O'Brien et al. found that $\Delta G_{ij}(n)$, the change in the Gibbs free energy associated with transitioning from peptide structure j with n peptides to a different type of peptide structure i, also with n peptides, is given by eq 2.

$$\Delta G_{ij}(n) = \frac{k_b T \phi}{V_c}(V_{ex}^i(n) - V_{ex}^j(n))$$

(2)

In eq 2, $V_{ex}^i(n)$ and $V_{ex}^j(n)$ are the volumes excluded to the crowders by the peptide structures i and j, ϕ is the crowder volume fraction, and V_c is the volume of a single crowder.[39] If $\Delta G_{ij}(n)$ is negative, then species i is more energetically favorable than species j and it is more likely that species i occupies a small enough volume to fit within the interstitial spaces of the crowders. If $\Delta G_{ij}(n)$ is positive, then species j is more energetically favorable than species i and it is more likely that species j occupies a small enough volume to fit within the interstitial spaces of the crowders.

O'Brien et al. also developed expressions for the volume excluded to the crowders by monomers, $V_{ex}^M(n)$, disordered aggregates, $V_{ex}^D(n)$, and beta sheets, $V_{ex}^\beta(n)$, of size n. These are given in eqs 3, 4, and 5, respectively.

$$V_{ex}^M(n) = \frac{4\pi n}{3}[(R_g + R_c)^3 - R_g^3]$$

(3)

$$V_{ex}^D(n) = \frac{4\pi}{3}[(nR_g + R_c)^3 - (nR_g)^3]$$

(4)

$$V_{ex}^\beta(n) = (l + 2R_c)(w + 2R_c)(h + 2R_c) - lwh$$
$$- \left(8R_c^3 - \frac{4}{3}\pi R_c^3\right)$$

(5)

The volume excluded to crowders by monomers in eq 3 is calculated by using the crowder radius R_c and approximating the peptide as a sphere with the peptide's radius of gyration R_g. In eq 4, the disordered aggregate is approximated as a spherical globule made of n peptides resulting in a larger sphere of radius nR_g. In eq 5, the β-sheet is approximated as a series of n connected rectangular parallelepipeds, each with length l, width w, and height h. For our calculations, we take these to be the average dimensions of a single $A\beta(16-22)$ peptide in a β-sheet

measured in our simulations to have length ~20 Å, width ~7.1 Å, and height ~4 Å.

Fibrillization Curve Fit and Parameters. In order to characterize the formation of fibrils, the number of peptides in fibrils at time t, $N_{fibril}(t*)$, vs reduced time was fit to eqs 6–11. These equations were derived by Cohen et al. using fixed point analysis to model fibrillization (in the absence of crowders) in terms of the microscopic processes of primary fibril nucleation, fibril elongation, and secondary nucleation.[40] By fitting our data on the number of peptides in fibrils as a function of time given an initial peptide concentration, c_0, to these six equations, we are able to extract the rate constants k_n the primary fibril nucleation rate which describes the formation of a fibril from solution, k_+ the fibril elongation rate which describes the addition of monomers to existing fibrils, and k_2 the secondary fibril nucleation rate which describes the formation of secondary fibrillar structures, in our case the addition of β-sheets, to the fibril.

$$\frac{N_{fibril}(t*)}{192} = 1 - \left(\frac{B_+ + A_+}{B_+ + A_+e^{\kappa t}}\right)\left(\frac{B_- + A_+e^{\kappa t*}}{B_- + A_+}\right)^{g_\infty^2/\kappa h_\infty} e^{-k_\infty t*}$$

(6)

$$\kappa = (2k_+k_2c_0^3)^{1/2}$$

(7)

$$A_\pm = \pm\frac{k_n}{2k_2c_0}$$

(8)

$$B_\pm = \left(\frac{1}{12} + \frac{k_n}{4k_2c_0}\right)^{1/2} \pm \left(\frac{1}{12} + \frac{k_n}{4k_2c_0} + \frac{k_n^2}{4k_2^2c_0^2}\right)^{1/2}$$

(9)

$$g_\infty = \left(2k_+c_0\left[\frac{k_2c_0^2}{3} + k_nc_0\right]\right)^{1/2}$$

(10)

$$h_\infty = \left(2k_+c_0\left[\frac{k_2c_0^2}{3} + k_nc_0 + \frac{k_n^2}{k_2}\right]\right)^{1/2}$$

(11)

In these equations, κ is an effective rate constant describing the secondary aggregation pathway comprised of secondary nucleation and fibril elongation, $A_\pm$, $B_\pm$, g_∞, and h_∞ are constants that are determined by the rate constants k_n, k_+, and k_2 as well as the initial peptide concentration c_0 of 5 mM. These equations are rearranged versions of the equations that appear in the paper by Cohen et al. so as to contain only the rate constants of interest and the initial monomer concentration. The average R_2 value for our curve fit of the number of peptides in fibrils vs reduced time to eqs 6–11 was 0.98. We have also calculated the lag time, t_{lag}, shown in eq 12, the critical primary fibril nucleation rate constant, k_{nc}, shown in eq 13, and the maximum fibril growth rate, r_{max}, shown in eq 14.

$$t_{lag} = \frac{\log(2k_2c_0/k_n) - e + 1}{\sqrt{2k_+k_2c_0^3}}$$

(12)

$$r_{max} = 192\sqrt{\frac{2k_+k_2c_0^3}{e^2}}$$

(13)

$$k_{nc} = \sqrt{\frac{k_+k_2c_0}{2e^2}}$$

(14)

The lag time is the amount of time before fibrillization begins, the maximal growth rate is the fastest fibril growth rate that occurs during the simulation, and the critical primary fibril nucleation rate constant is the value for the primary fibril nucleation rate constant above which there is no lag phase. Additionally, we look at the nucleation time, which we define to be the first time point that has 20 consecutive nonzero values for the number of peptides in fibrils following it. Twenty consecutive time points equates to ∼56 reduced time units. Here we use the term nucleation time in the place of lag time because our simulations operate above the supercritical peptide concentration and there is no lag time as calculated by eq 12.

■ RESULTS

Aggregation in the Presence of Crowders. Figure 1 shows snapshots from a simulation of 192 $A\beta(16-22)$ peptides
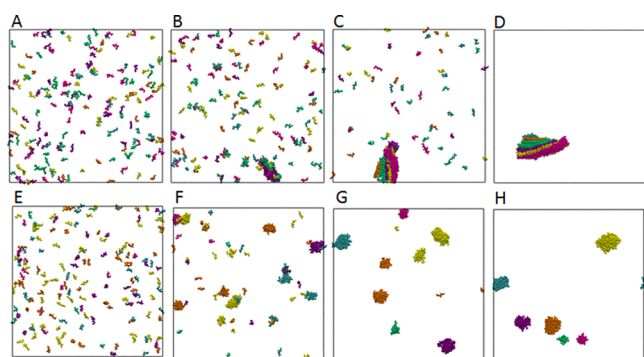

Figure 1. Snapshots of simulation progress for simulations. Top row: no crowders at $t^* =$ (A) 0, (B) 400, (C) 1100, and (D) 2000. Bottom row: 5 Å crowders at crowder volume fraction $\phi = 0.20$ at $t^* =$ (E) 0, (F) 90, (G) 220, and (H) 270.

in the absence of crowders (A−E) and in the presence of crowders (F−J) with crowder volume fraction $\phi = 0.20$ and crowder diameter 5 Å (crowders have been removed for clarity). The peptide concentration is 5 mM, and the reduced temperature is $T^* = 0.193$. In the simulation with no crowders, the peptides have been colored so that all of the peptides in a given β-sheet at the conclusion of the simulation have the same color and in the simulation with crowders the peptides have been colored so that all of the peptides in a given fibril at the conclusion of the simulation have the same color. At $t^* = 0$ (Figure 1A and E), the initial peptide configuration for both simulations is random coils. In the simulation with no crowders, some peptides begin to interact transiently but do not form a stable fibril nucleus until $t^* = 400$ (Figure 1B). The fibril nucleus is composed of two stable β-sheets colored green and light blue. At $t^* = 400$, the fibril has begun to elongate through monomer addition at the ends of the fibril; each β-sheet has lengthened, increasing the overall size of the fibril. At $t^* = 1100$ (Figure 1C), three additional β-sheets have attached themselves to the fibril, resulting in a much larger five-sheet fibril. Finally, at $t^* = 2000$ (Figure 1D), all of the peptides in the simulation have integrated themselves into a single large fibril composed of six β-sheets. The simulation with crowders begins to form small oligomers very early in the simulation at $t^* = 90$ (Figure 1F). Soon after, the previously formed oligomers begin to rearrange themselves from disordered conformations into β-sheets and small fibrils while new oligomers are formed from the remaining free monomers. At $t^* = 220$ (Figure 1G), almost

all of the free monomers have been integrated into an oligomer or fibril and they continue to reorganize from disordered conformations to β-sheets. Finally, at $t^* = 270$ (Figure 1H), all of the disordered structures have reorganized into β-sheets, resulting in six small fibrils.

By comparing the time scales for these two representative simulations, we can see that fibrillization is complete at $t^* = 2000$ for the simulation with no crowders and at $t^* = 270$ for the simulation with crowders. It is evident that the presence of crowders not only dramatically decreases the time scale of aggregation but, as can be seen from the snapshots, the aggregation mechanisms are different. In the simulation without crowders, a single long fibril forms through nucleated polymerization. In contrast, the simulation with crowders results in six small fibrils that form from smaller disordered oligomers characteristic of nucleated conformational conversion. These oligomers are initially disordered because the peptides are rapidly forced together by depletion forces. Since the peptides are forced together so quickly, they do not have the ability to orient themselves into a more favorable structure like a β-sheet. It is interesting to note that, in the absence of fibrils, one large fibril is formed at $t^* = 2000$ but with crowding agents, six small fibrils form after only a fraction of the simulation time. It is unlikely that these six small fibrils would combine into a single large fibril if the simulation was run until $t^* = 2000$. These small fibrils are very stable and energetically favorable, and while a few of them may combine to make a slightly larger fibril, we expect that much more computational time would be needed to observe a single large fibril forming from the smaller six. We speculate that this increase in the number of individual fibrils may be a general consequence of very crowded conditions. Support for this idea comes from simulations by Magno et al., who found that the number of supercritical oligomers (prefibrillar structures) increases with crowder concentration.[23]

As has been pointed out by other investigators, the dramatic effect of crowding on peptide oligomerization and fibrillization can be understood in part by appealing to the concept of depletion forces.[22,41] The depletion forces acting in our simulations can be approximated by adapting the expression introduced by Asakura and Oosawa to this case. The depletion potential, $U(r)$, between two peptides whose centers of mass are separated by distance r in the presence of crowders is[42]

$$U(r) = -\frac{\phi}{16R_c{}^3}k_BT[2(R_c + R_g)^3 - 3(R_c + R_g)^2 r - r^3]$$

(15)

where ϕ is the crowder volume fraction, R_c is the crowder radius, and R_g is the radius of gyration of the peptide. This equation is only valid for $R_c < r < R_g + R_c$, and although it is typically applied when $R_c \ll R_g$, it provides a reasonable qualitative comparison of depletion forces for different crowder sizes. Since all of our simulations are run at the same temperature, simulation box volume, and peptide radius of gyration, the depletion potential will only change when the crowder volume fraction or the crowder radius changes. As the crowder volume fraction increases, the depletion potential increases. As the crowder radius increases (at constant crowder volume fraction), the strength of the depletion potential decreases, although the range increases. The increased strength of the depletion potential for smaller crowders is what drives oligomerization, and by extension fibrillization, to occur at an
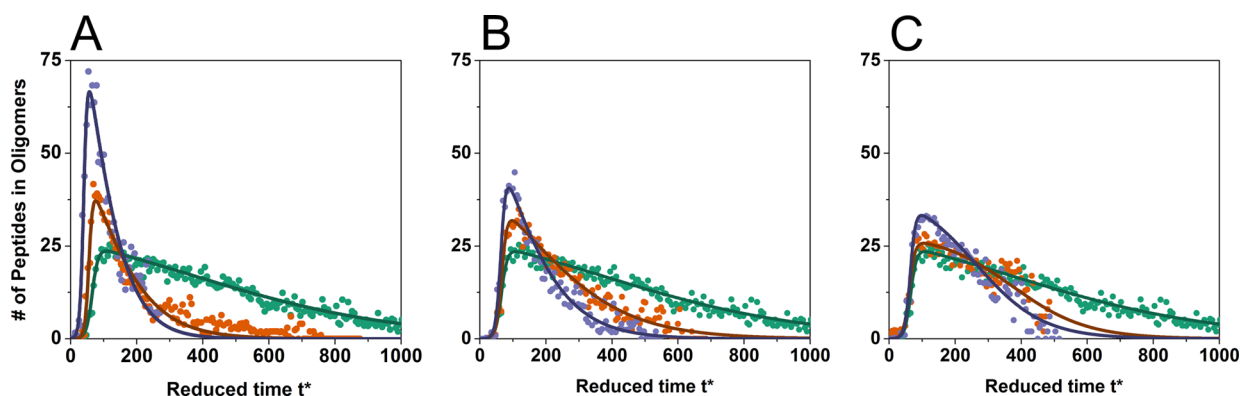
13518

dx.doi.org/10.1021/jp508970q | *J. Phys. Chem. B* 2014, 118, 13513−13526

Figure 2. Number of peptides in oligomers vs reduced time for (A) 5 Å crowders, (B) 20 Å crowders, and (C) 40 Å crowders at ϕ = 0.00 (green), 0.10 (orange), and 0.20 (purple) along with curve fits to an asymmetric double sigmoidal function.

Table 1. Oligomer Growth Rate, Maximum Number of Peptides in Oligomers, and Oligomer to Fibril Conversion Time for Crowder Volume Fractions ϕ = 0.00, 0.10, and 0.20 and Crowder Diameters 5, 20, and 40 Å and Total Crowder Surface Area

		crowder size, crowder volume fraction, and total crowder surface area					
		D = 40 Å	D = 40 Å	D = 20 Å	D = 20 Å	D = 5 Å	D = 5 Å
	no crowders	ϕ = 0.10	ϕ = 0.20	ϕ = 0.10	ϕ = 0.20	ϕ = 0.10	ϕ = 0.20
kinetic parameters	ϕ = 0.00	96×10^{-4} Å^2	192×10^{-4} Å^2	192×10^{-4} Å^2	384×10^{-4} Å^2	786×10^{-4} Å^2	1536×10^{-4} Å^2
growth rate (peptides time^{-1})	0.61 ± 0.30	0.74 ± 0.42	1.06 ± 0.68	1.00 ± 0.54	1.43 ± 0.37	1.48 ± 0.47	3.21 ± 1.06
maximum number of peptides (peptides)	23.61 ± 4.30	25.74 ± 3.44	33.23 ± 4.38	31.84 ± 3.37	40.63 ± 4.49	37.20 ± 5.97	66.55 ± 5.00
conversion time (time)	600.67 ± 187.58	346.58 ± 67.78	249.89 ± 11.81	250.08 ± 42.67	145.44 ± 31.46	137.84 ± 40.74	95.92 ± 12.80

accelerated rate compared to simulations in the absence of crowders.

Effects of Crowding on Oligomerization. Oligomerization is the first step in the aggregation process for Aβ(16−22). Figure 2 shows the number of peptides in oligomers vs reduced time for crowder volume fractions ϕ = 0.00 (no crowders), 0.10, and 0.20 at crowder diameters (A) 5 Å, (B) 20 Å, and (C) 40 Å. The number of peptides in oligomers increases sharply as peptides begin to interact and then gradually decreases as the oligomers are converted to fibrils over time.

We begin our analysis of the oligomerization data by examining the rate of oligomer growth. Table 1 summarizes the results for the oligomer growth rate, maximum number of peptides in oligomers, and oligomer to fibril conversion time at crowder volume fractions ϕ = 0.00, 0.10, and 0.20 and crowder diameters 5, 20, and 40 Å. A useful measure of crowding conditions, in addition to crowder volume fraction and diameter, is the total crowder surface area, listed below the corresponding crowder volume fraction and crowder diameter in the table. Total crowder surface area is simply the surface area of a single crowder multiplied by the number of crowders in the simulation. The first row of Table 1 shows the oligomer growth rate. At a constant volume fraction, decreasing the diameter of the crowders increases the oligomer growth rate. If the crowder diameter is held constant, increasing the crowder volume fraction increases the oligomer growth rate. The table shows that, as the total crowder surface area increases, the growth rate increases monotonically. The highest growth rate is 3.21 peptides added per unit time for 5 Å crowders at a crowder volume fraction of ϕ = 0.20 having a total crowder surface area of 0.1536 Å^2. This growth rate is more than 5 times greater than that in the absence of crowders. The increase in oligomer growth rate with crowder volume fraction can be attributed to

an increase in the effective concentration of the peptides. When crowders are added to the simulation, they exclude volume to the peptides, making a large portion of the system inaccessible. The increase in oligomer growth rate when decreasing the crowder diameter can be attributed to the increase in depletion forces. As the size of the crowders decreases at a fixed volume fraction, the magnitude of the depletion forces increases, further enhancing peptide−peptide interactions. Thus, as either the crowder volume fraction increases or the crowder diameter decreases, the peptides have a higher propensity to associate, leading to a higher oligomer growth rate.

At some point during oligomerization, a fibril nucleates and the number of peptides in oligomers begins to decline as they are integrated into fibrils. This transition occurs when the number of peptides in oligomers reaches its maximum value. The second row of Table 1 shows the maximum number of peptides in oligomers. At a constant volume fraction, decreasing the diameter of the crowders increases the maximum number of peptides in oligomers. If the crowder diameter is held constant, increasing the crowder volume fraction increases the maximum number of peptides in oligomers. Just like the oligomer growth rate, there is a monotonically increasing relationship between the maximum number of peptides in oligomers and the total crowder surface area. At the highest total crowder surface area, which corresponds to 5 Å crowders and crowder volume fraction ϕ = 0.20, the maximum number of peptides in oligomers is 66.55, which is almost triple the amount in the absence of crowders. Similar to the oligomer growth rate, increasing the crowder volume fraction and decreasing the crowder size increases the maximum number of peptides in oligomers. Once the peptides form an oligomer, they are in a more energetically favorable state because they occupy less space than the equivalent number of free monomers. For this

reason, the peptides do not dissociate, leading to a higher maximum number of peptides in oligomers.

After the number of peptides in oligomers peaks, the oligomers begin to convert to fibrils. We characterize this process by calculating the oligomer to fibril conversion time. The third row of Table 1 shows the oligomer to fibril conversion time. At a constant crowder volume fraction, decreasing the diameter of the crowders decreases the oligomer to fibril conversion time. If the crowder diameter is held constant, increasing the crowder volume fraction decreases the oligomer to fibril conversion time. As the total crowder surface area increases, the oligomer to fibril conversion time decreases exponentially to its lowest value: 95.92 time units for 5 Å crowders at a crowder volume fraction of $\phi = 0.20$. Since fibrils occupy even less space than an equivalent number of peptides in an oligomer, they are more energetically favorable, providing a more thermodynamically stable structure than an oligomer. Larger depletion forces and a higher effective concentration make the oligomer to fibril conversion time shorter.

Summarizing thus far, the presence of crowders tends to increase oligomer formation. Increasing crowder volume fraction and decreasing crowder diameter increases the growth rate of oligomers and the maximum number of peptides in oligomers but decreases the oligomer to fibril conversion time. Although crowders promote rapid oligomerization early in the simulation, they also drive oligomers to form fibrils at a faster rate.

Effects of Crowding on Small Oligomer Formation. Since small oligomers have been identified as toxic agents in Alzheimer's disease, the dependence of the number of peptides in dimers, trimers, tetramers, pentamers, and hexamers on crowder diameter and crowder volume fraction is of interest. Here we focus on 5 and 40 Å crowders to see how the smallest and largest crowders impact small oligomer formation.

The oligomerization mechanisms observed in our simulations can be described most simply in terms of a step-growth mechanism. In a step-growth mechanism, monomers come together one by one to first form dimers, then trimers, then tetramers, etc., which means that the maximum number of peptides in dimers is greater than the maximum number of peptides in trimers and so on. In other words, the smaller oligomers need to be formed before additional peptides can be added.

To begin our analysis, we plot the curve fits to the number of peptides in dimers, trimers, tetramers, pentamers, and hexamers from our simulations vs reduced time using the asymmetric double sigmoidal function described in the Methods section. Figure 3 shows the number of peptides in dimers through hexamers vs reduced time for simulations with no crowders. The same data is shown in Figure 4 for $\phi = 0.10$ and in Figure 5 for $\phi = 0.20$, with crowders of diameter 40 Å (A), 20 Å (B), and 5 Å (C). Table 2 shows a summary of the fraction of oligomeric peptides that are dimers and hexamers at crowder volume fractions $\phi = 0.00$, 0.10, and 0.20 and crowder diameters 5, 20, and 40 Å. In the first row of Table 2, 40 Å crowders have a larger fraction of oligomeric peptides in dimers than for 20 and 5 Å crowders. However, simulations with no crowders have an even higher fraction of oligomeric peptides in dimers than simulations with 40 Å crowders. This indicates that the addition of crowders to a no-crowder simulation decreases the dimer content regardless of the properties of the crowders. It should be noted that, for a given crowder volume fraction, larger crowders will have the smallest deviation from the no-
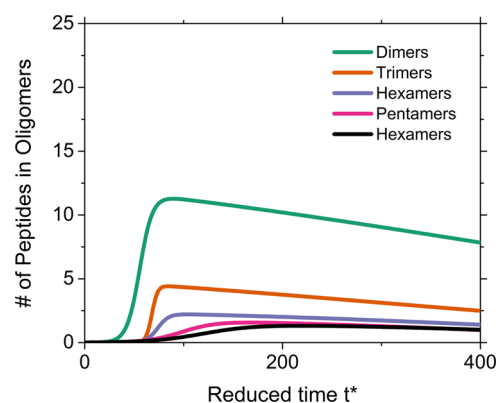

Figure 3. Number of peptides in small oligomers of different sizes vs reduced time for no crowders.

crowder results due to their smaller surface to volume ratio. When comparing results from our simulations at the same crowder volume fractions but different crowder diameters, the 40 Å crowders have the highest propensity to favor dimer formation. In the second row of Table 2, the 5 Å crowders have a higher fraction of oligomeric peptides that are hexamers than the 20 and 40 Å crowder simulations.

Here we compare our conclusions from Table 2 to the free energy analysis introduced by O'Brien et al. presented in the Methods section.[22] The data presented in Table 2 shows that the fraction of oligomeric peptides in dimers at a fixed volume fraction is highest for simulations with 40 Å crowders, and the fraction of oligomeric peptides in hexamers is highest for simulations with 5 Å crowders. In order to interpret the change in free energy associated with transitioning from a monomer to an oligomer in the presence of 40 Å crowders, we will use eq 3 for monomers with eq 4 for disordered aggregates rather than eq 5 for beta sheets because the peptides are typically in a more compact state rather than an extended confirmation when confined in the space between 40 Å crowders. Figure 6 shows a plot of the difference in free energy between a disordered aggregate of size n and n free monomers ΔG_{DM} vs the number of peptides n for crowder diameter 40 Å predicted by eqs 2–4 at crowder volume fractions $\phi = 0.00$, 0.05, 0.10, 0.15, and 0.20. We have included additional values for the crowder volume fraction beyond what we simulated to provide clarity. The negative values of ΔG_{DM} for $n = 2$, 3, and 4 peptides and positive values for $n = 5$ and 6 peptides for the 40 Å crowders case suggests that the formation of disordered dimers, trimers, and sometimes tetramers is energetically favorable compared to the formation of larger pentamers and hexamers when compared to an equivalent number of free monomers.

Our result that 40 Å crowders favor the formation of dimers, trimers, and tetramers and that the 5 Å crowders favor the formation of pentamers and hexamers can be understood on the basis of the following arguments. We believe that the size of the interstitial spaces created by the 40 Å crowders, (as compared to the smaller size interstitial spaces created by the 5 Å crowders) is commensurate with the sizes of dimers, trimers, and tetramers and hence favors their formation. We have come to this conclusion based on the fact that negative values of $\Delta G_{ij}(n)$ in eq 2 mean that the oligomer structure is energetically favorable when surrounded by crowders and occupies a volume small enough that crowders do not need to be displaced when the oligomer is present. In addition, since the depletion forces are weakest for the 40 Å crowders and the
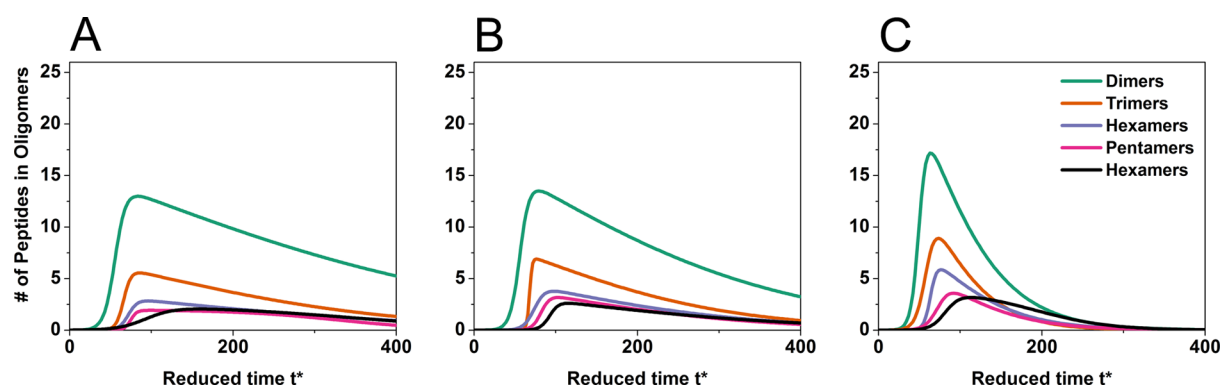
Figure 4. Number of peptides in small oligomers of different sizes vs reduced time at $\phi = 0.10$ for (A) 40 Å crowders, (B) 20 Å crowders, and (C) 5 Å crowders.

Figure 5. Number of peptides in small oligomers of different sizes vs reduced time at $\phi = 0.20$ for (A) 40 Å crowders, (B) 20 Å crowders, and (C) 5 Å crowders.
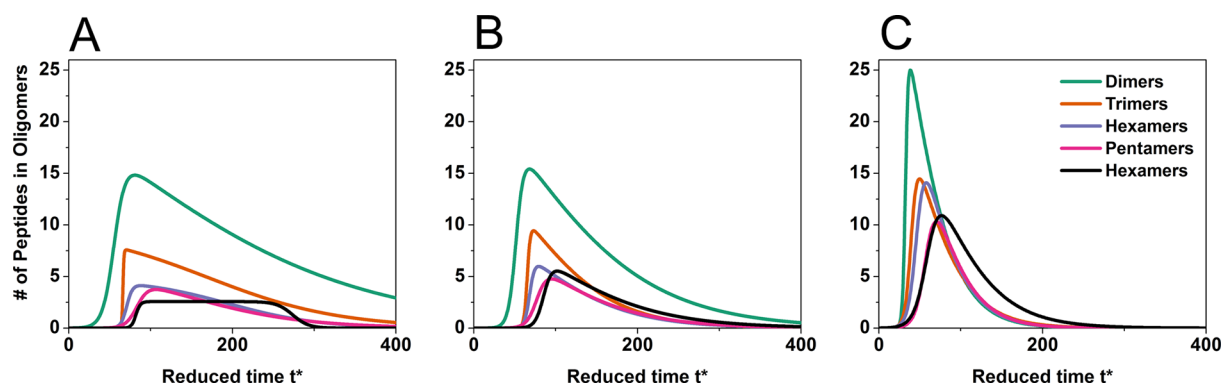
Table 2. Maximum Fraction of Oligomeric Peptides in Dimers and in Hexamers for Crowder Volume Fractions $\phi = 0.00$, 0.10, and 0.20 and Crowder Diameters 5, 20, and 40 Å and Total Crowder Surface Area

		crowder size, crowder volume fraction, and total crowder surface area					
		$D = 40$ Å	$D = 40$ Å	$D = 20$ Å	$D = 20$ Å	$D = 5$ Å	$D = 5$ Å
	no crowders	$\phi = 0.10$	$\phi = 0.20$	$\phi = 0.10$	$\phi = 0.20$	$\phi = 0.10$	$\phi = 0.20$
small oligomer fractions	$\phi = 0.00$	96×10^{-4} Å^2	192×10^{-4} Å^2	192×10^{-4} Å^2	384×10^{-4} Å^2	786×10^{-4} Å^2	1536×10^{-4} Å^2
dimer:total oligomer fraction	0.54	0.52	0.47	0.44	0.39	0.44	0.33
hexamer:total oligomer fraction	0.06	0.10	0.08	0.09	0.13	0.08	0.15

interstitial spaces are of limited size, there is little in the way of driving force to create larger oligomers. This is consistent with the following ideas which were mentioned earlier. If the oligomer occupies approximately the same volume or less than the interstitial spaces between the crowders, it is energetically favorable because the crowders do not need to move to accommodate the oligomer. If the volume of the oligomer is greater than the interstitial space, it becomes energetically unfavorable because the oligomer no longer fits neatly into the space and the crowders must be moved in order to accommodate the oligomer. In the case of the smaller 5 Å crowders, the interstitial spaces created are so small that no particular size oligomer is favored. However, the depletion forces are quite sizable, so that once any oligomer forms it tends to grow larger due to the large depletion forces. The latter effect can be seen in the following analysis of our simulations with 5 Å crowders.

To continue our free energy analysis, we now examine the case of 5 Å crowders. In order to interpret the change in free energy associated with the transition from a monomer to an

oligomer in the presence of 5 Å crowders, we will use eq 3 for monomers with eq 5 for β-sheet aggregates rather than eq 4 for disordered aggregates. This is because the peptides typically adopt a more extended conformation when surrounded by 5 Å crowders than by the larger crowders, since the small crowders can sit closer to the peptide backbone. Applying eqs 2, 3, and 5, we arrive at Figure 7 which shows the difference in free energy between a β-sheet of size n and n free monomers $\Delta G_{\beta M}$ vs the number of peptides n at crowder volume fraction $\phi = 0.20$. For each crowder diameter, increasing the number of peptides n makes $\Delta G_{\beta M}$ more negative, favoring the formation of a β-sheets over free monomers. Although the formation of larger aggregates is favorable for all sizes of crowders, the favorability of β-sheet formation increases more rapidly as the crowder volume fraction increases for the 5 Å crowders than for 20 and 40 Å crowders because the change in free energy $\Delta G_{\beta M}$ is significantly more negative (data not shown). Since small crowders create a larger depletion force between peptides, the attractive force promotes the formation of aggregates in favor of free monomers.
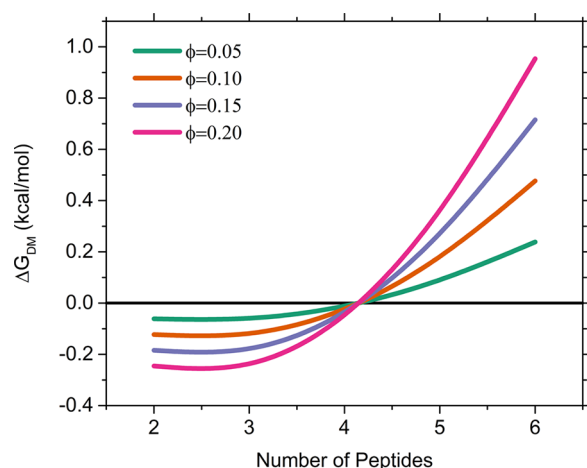
Figure 6. Difference in free energy between a disordered aggregate and free monomers vs number of peptides for crowder volume fractions ϕ = 0.20, 0.15, 0.10, and 0.05 with a crowder diameter of 40 Å.
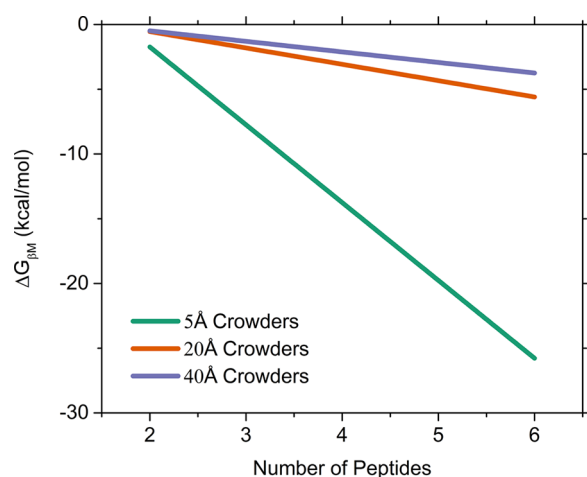

Figure 7. Difference in free energy between a β sheet and free monomers vs the number of peptides at crowder volume fraction ϕ = 0.20 for crowder diameters 5, 20, and 40 Å.

Effects of Crowding on Fibrillization. We now turn our attention to the formation of fibrillar structures which occurs after the oligomers have formed. Some of the mechanisms

suggested to govern fibril formation are nucleated polymerization in which fibril growth does not occur until a nucleus is formed and growth occurs via monomer addition to the fibril or nucleated conformational conversion in which monomers rapidly aggregate into oligomers, and then convert to fibrils over time.[43,44] Figure 8 shows the number of peptides in fibrils vs reduced time for crowder volume fractions ϕ = 0.00 (no crowders), 0.10, and 0.20 at crowder diameters (A) 5 Å, (B) 20 Å, and (C) 40 Å. The fibrils formed in the simulations at ϕ = 0.00, i.e., no crowders, have a relatively linear growth rate over the 1200 reduced time units in Figure 8. However, once crowders are added, as in the ϕ = 0.10 and 0.20 simulations, rapid fibrillization occurs at earlier times.

Table 3 summarizes the results for the kinetic constant parameters for the fibrillization fit to the model of Cohen et al. as described in the Methods section: the primary fibril nucleation rate constant, critical primary fibril nucleation rate constant, maximum fibril growth rate, fibril elongation rate constant, and the secondary fibril nucleation rate constant at crowder volume fractions ϕ = 0.00, 0.10, and 0.20 and crowder diameters 5, 20, and 40 Å. The first row of Table 3 shows the primary fibril nucleation rate constant, k_n, which describes the formation of a fibril nucleus from a solution of monomers. All of the simulations have primary fibril nucleation rate constants that fall between 0.20 and 0.25 M^{-1} s^{-1}, except for the simulations with a crowder volume fraction of ϕ = 0.20 with 5 Å crowders, which has a primary fibril nucleation rate constant of 0.46 M^{-1} s^{-1}. The highest rate of primary fibril nucleation occurs for the highest crowder volume fraction with the smallest crowders. This indicates that the large depletion forces under these conditions force nucleation to occur much more rapidly, causing multiple small fibrils to form rather than a single large fibril, as shown in Figure 1.

The second row of Table 3 shows the critical primary fibril nucleation rate constants, k_{nc}, which can be compared to the primary fibril nucleation rate constant. The critical primary fibril nucleation rate constant is the value for the primary fibril nucleation rate constant above which there is no lag phase. In every case, the primary fibril nucleation rate constant is greater than the critical value, confirming that there is no lag phase in our simulations. Our hypothesis as to why there is no lag phase in our simulations is that there is minimal, if any, monomer dissociation from oligomers and fibrils, indicating that both structures are more energetically favorable than a free monomer
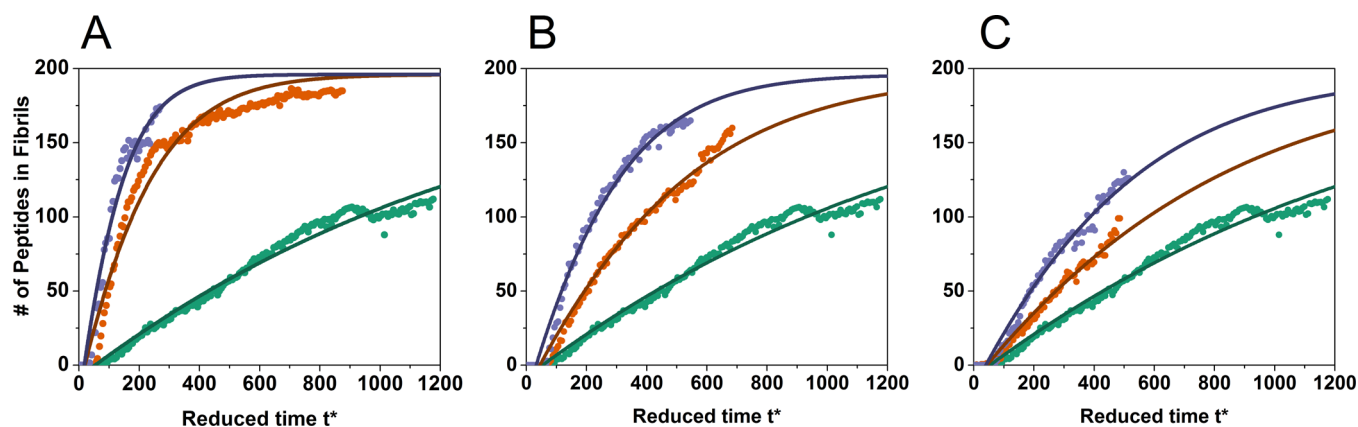

Figure 8. Number of peptides in fibrils vs reduced time for (A) 5 Å crowders, (B) 20 Å crowders, and (C) 40 Å crowders at ϕ = 0.00 (green), 0.10 (orange), and 0.20 (purple).

Table 3. Fibril Primary Nucleation Rate, Critical Nucleation Rate, and Maximum Growth Rate, Elongation Rate, and Secondary Nucleation Rate for Crowder Volume Fractions ϕ = 0.00, 0.10, and 0.20 and Crowder Diameters 5, 20, and 40 Å and Total Crowder Surface Area Obtained by Fitting Simulation Data to Eqs 6−11

		crowder size, crowder volume fraction, and total crowder surface area					
		$D = 40$ Å	$D = 40$ Å	$D = 20$ Å	$D = 20$ Å	$D = 5$ Å	$D = 5$ Å
	no crowders	$\phi = 0.10$	$\phi = 0.20$	$\phi = 0.10$	$\phi = 0.20$	$\phi = 0.10$	$\phi = 0.20$
kinetic parameters	$\phi = 0.00$	96×10^{-4} Å^2	192×10^{-4} Å^2	192×10^{-4} Å^2	384×10^{-4} Å^2	786×10^{-4} Å^2	1536×10^{-4} Å^2
k_n (M^{-1} time^{-1})	0.21 ± 0.06	0.25 ± 0.10	0.24 ± 0.06	0.20 ± 0.09	0.25 ± 0.05	0.25 ± 0.09	0.46 ± 0.18
k_{nc} (M^{-1} time^{-1})	0.03 ± 0.01	0.04 ± 0.01	0.07 ± 0.01	0.07 ± 0.01	0.12 ± 0.02	0.15 ± 0.03	0.26 ± 0.02
r_{max} (peptides time^{-1})	0.05 ± 0.02	0.08 ± 0.02	0.13 ± 0.02	0.13 ± 0.02	0.24 ± 0.04	0.29 ± 0.05	0.51 ± 0.04
k_+ (M^{-1} time^{-1})	1.40 ± 0.44	2.17 ± 0.35	3.31 ± 0.40	3.42 ± 0.43	5.85 ± 0.78	13.48 ± 2.94	11.38 ± 2.03
k_2 (M^{-2} time^{-1})	1.45 ± 0.46	2.53 ± 0.66	4.03 ± 0.64	3.97 ± 0.64	7.41 ± 1.58	4.87 ± 4.55	17.53 ± 10.33

and that we are operating above the supercritical peptide concentration as described by Powers and Powers.[45] The maximum fibril growth rate, r_{max}, for each type of simulation is shown in row three of Table 3. The maximum fibril growth rate has a monotonically increasing trend with total crowder surface area. Although the primary nucleation rate is approximately the same for all simulations, except at $D = 5$ Å and $\phi = 0.20$, we can see that the maximum growth rate does in fact increase with increasing crowder surface area. This trend indicates that, although primary nucleation occurs at approximately the same rate for all conditions, the growth rate directly following nucleation increases with increasing crowder surface area.

Next we look at the fibril elongation rate, k_+, which describes the rate of fibril growth through monomer addition to the ends of the fibril and the rate of secondary fibril nucleation, k_2, which in our simulations is the rate of addition of a new β-sheet to a fibril. The fourth and fifth rows of Table 3 show the fibril elongation rate constant and secondary fibril nucleation. Smaller crowder diameters and larger crowder volume fractions increase both the fibril elongation rate and secondary nucleation rate. As the total surface area of the crowders increases, the fibril elongation rate constant and secondary nucleation rate also increase monotonically. The exception to the monotonically increasing trend is the $D = 5$ Å, $\phi = 0.20$ case. If a linear trend were to apply to these simulations, we would expect an elongation rate constant of ~ 25 M^{-1} s^{-1} and a secondary nucleation rate constant of ~ 10 M^{-2} s^{-1}, but instead, they are 11.38 M^{-1} s^{-1} and 4.87 M^{-2} s^{-1}, respectively. We are unsure why this deviation occurred, but it is possible that it is because we need a more comprehensive equation to describe fibrillization that includes mechanisms beyond primary nucleation, secondary nucleation, and elongation.

The fastest fibril growth rate in our simulations occurs at a crowder volume fraction of $\phi = 0.20$ and a diameter of 5 Å where primary and secondary nucleation are very high. We attribute the high rates of primary and secondary nucleation to the very high depletion forces that occur under these conditions. A high rate of primary and secondary nucleation should lead to the formation of a large number of fibrils made of many β-sheets. This behavior is indicative of nucleated conformational conversion in which the peptides rapidly form disordered oligomers, and then reorganize over time to form fibrils. This is consistent with the snapshots of our simulations in Figure 1H for a crowder volume fraction of $\phi = 0.20$ and 5 Å crowders. As the crowder volume fraction decreases and the size of the crowders increases, the depletion forces become less prominent and the aggregation mechanism begins to shift toward slow ordered fibril growth characteristic of nucleated polymerization. Nucleated polymerization would have lower values of primary and secondary nucleation relative to fibril elongation because nucleation occurs much less often than in simulations with higher depletion forces. If nucleation occurs at a lower rate and fibril elongation dominates, we would expect a smaller number of longer fibrils and that is exactly what we saw in our simulations in Figure 1E.

Nucleation time is the amount of time it takes until the first fibril begins to form. We define the nucleation time as the reduced time at which there are 20 consecutive nonzero values for the number of peptides in fibrils. Without crowders, fibril nucleation occurs after 38.0 reduced time steps. The fibril nucleation time shows no particular trend with increasing crowder volume fraction or crowder diameter for 20 and 40 Å crowders, varying between 31.5 and 41.2 reduced time steps for 20 Å crowders and 34.7 and 44.4 reduced time steps for 40 Å crowders (data not shown). This indicates that the presence of 20 or 40 Å crowders does not provide enough excluded volume to force peptides down an aggregation pathway consistently and that the nucleation time is random and most likely dependent on the initial spatial distribution of peptides. We did not observe the decrease in nucleation time at high crowder volume fractions mentioned in the Introduction. Our explanation for why we did not observe this behavior is that our peptide does not need to fold in order to be a part of a fibril. High crowder volume fractions and small crowders could prevent the peptides from adopting the proper conformation to be integrated into a fibril, but in our simulations, there is no folding because $A\beta(16-22)$ is only 7 residues long, so this effect is not present. Additionally, the crowder volume fractions we studied may not be large enough to see the delay in nucleation time observed by others.

■ DISCUSSION AND CONCLUSIONS

Using the combination of DMD and our PRIME20 force field, we have been able to simulate systems of coarse grained proteins that have realistic geometry and energetic parameters along with crowding spheres up to realistic volume fractions. Although previous studies have been performed on similar systems, we are not aware of any that match the scale and realism of the species involved in the simulations. The systems contained 192 $A\beta(16-22)$ peptides and crowders of diameters 5, 20, and 40 Å, represented here by simple hard spheres, at crowder volume fractions of $\phi = 0.00$, 0.10, and 0.20. Our results show that both crowder volume fraction and size have a large impact on fibril and oligomer formation. The addition of crowders to a simulation without crowders increases the rate of oligomer formation and the peak number of oligomers that

form. As the crowder volume fraction increases or the crowder diameter decreases, the increase in oligomer formation is accompanied by a shift from a slow ordered formation of oligomers, similar to nucleated polymerization, to a fast collapse and subsequent rearrangement that leads to the high maximum number of peptides in oligomers as is characteristic of nucleated conformational conversion. The rate of conversion from oligomers to fibrils also increases, giving rise to an increased rate of fibril growth. On the basis of our analysis, it appears there is not an abrupt transition from nucleated polymerization to nucleated conformational conversion while increasing crowder volume fraction or decreasing crowder size; rather, the mechanism governing fibrillization changes gradually with the simulation conditions. In all cases, larger volume fractions and smaller crowders provide the largest enhancement of oligomerization and fibrillization. These results agree with those of O'Brien et al. in that adding crowders of any size or concentration to the simulation will enhance aggregation and as the size of the crowders increases the level of aggregation enhancement is diminished.[22] Although crowding is also expected to impact oligomerization and fibrillization through changes in peptide diffusion and viscosity, we have not analyzed those effects here.

We have also presented a free energy analysis of the formation of dimers, trimers, tetramers, pentamers, and hexamers in the presence of crowders. In our simulations, the 40 Å crowders have interstitial spaces that are large enough to easily accommodate the dimers and therefore stabilize these oligomers, allowing them to persist longer relative to trimers, tetramers, pentamers, and hexamers when compared to systems of equivalent crowder volume fractions but different crowder diameters. The depletion forces from the 5 Å crowders are so great that the largest oligomers, in our case hexamers, are the most energetically favorable. Our analysis showed that in the presence of crowders it is possible for specific oligomers to be more energetically favorable than free monomers because they allow the peptides to adopt more compact conformations. This idea agrees with Munishkina et al. and their idea that, in the presence of crowders, specific oligomer and fibril aggregation pathways are preferred because of the favorability of specific peptide structures and the fact that they may be more energetically stable than others.[26]

Since Aβ fibrillization is thought to be a reaction-limited process, crowding should increase aggregation and that trend was observed.[17] One trend we did not observe in our simulations is the increase in fibrillization lag time associated with very high crowder volume fractions. We surmise that we did not observe this behavior because our peptide does not need to fold in order to be a part of a fibril. High crowder volume fractions and small crowders could prevent the peptides from adopting the proper conformation to be integrated into a fibril, but in our simulations, there is no folding because Aβ(16−22) is only seven residues long, so this effect is not present. Additionally, the crowder volume fractions we studied may not be large enough to see the delay in nucleation time predicted by Zimmerman and Minton and observed in experiment by Cabaleiro-Lago et al. and observed in simulation by Co et al.[8,24,25]

Although the combination of DMD and our intermediate resolution protein model, PRIME20, has allowed us to simulate the aggregation of a large number of peptides up to physiologically relevant conditions, there are some inherent limitations to our approach. Since the peptide studied is very short, only seven residues, we are not able to get a picture of how the competition between folding and aggregation changes in the presence of crowders. In the future, we hope to examine a longer protein sequence to focus on the effects of protein folding in addition to aggregation. Although we are unable to include hydrodynamic interactions in our DMD simulations, we believe that their inclusion would likely enhance the rate of oligomer and fibril formation beyond what we reported, since long-range hydrodynamic interactions typically reduce protein diffusion. In addition, since the peptide we are considering does not fold, intrapeptide hydrodynamic interactions would not come into play. Additionally, the model for the crowders that we have used here only takes crowder volume exclusion into account and does not capture the effects of nonspecific attractive interactions that may exist between proteins and crowders. A more detailed model might include these interactions to address how they might change the influence of crowding on aggregation. Finally, a more complex crowder geometry might be necessary to increase the accuracy of our simulations. We have limited our study to spherical crowders, but crowders represented as sphereocylinders, polymer chains, or coarse-grained representations of real crowding molecules might increase the relevance of our simulations. In a forthcoming study, we will examine how the addition of attractive crowders to a system of peptides affects aggregation and how different types of crowder−peptide interactions change the behavior of the system. We predict that the complex interplay between enthalpic and entropic effects imparted by attractive crowders should have a much different effect on aggregation than hard-core crowders, as shown by Kim and Mittal and Sapier and Harries.[46,47] Strongly attractive crowders would likely diminish the formation of oligomers and fibrils, counteracting the aggregation enhancement due to hard-core crowders shown in this paper.

The major conclusions in our paper are not sensitive to our definition of fibrils and oligomers. For example, our definition of an oligomer requires that at least two peptides share a side chain contact or a hydrogen bond. We considered breaking this into two classes of oligomer, disordered (primarily side chain contacts between chains) or ordered (β-sheet structure), but in these simulations disordered oligomers are very short-lived and needlessly complicate the discussion. A change in the definition of oligomer, e.g., requiring more hydrogen bonds, would simply shift the curves to a later point in time as the ultimate structures formed are the same. The values of our calculated parameters would change slightly, but the overall trends would be preserved.

■ AUTHOR INFORMATION

Corresponding Author
*E-mail: hall@ncsu.edu. Phone: 1-919-515-3571. Fax: 1-919-515-3463.
Notes
The authors declare no competing financial interest.

■ ACKNOWLEDGMENTS

■ REFERENCES

(1) Chiti, F.; Dobson, C. M. Protein Misfolding, Functional Amyloid, and Human Disease. *Annu. Rev. Biochem.* **2006**, *75*, 333−366.

(2) Lambert, M.; Barlow, A.; Chromy, B.; Edwards, C.; Freed, R.; Liosatos, M.; Morgan, T.; Rozovsky, I.; Trommer, B.; Viola, K.; et al. Diffusible, Nonfibrillar Ligands Derived from A Beta(1−42) are Potent Central Nervous System Neurotoxins. *Proc. Natl. Acad. Sci. U. S. A.* **1998**, *95*, 6448−6453.

(3) Gasser, B.; Saloheimo, M.; Rinas, U.; Dragosits, M.; Rodriguez-Carmona, E.; Baumann, K.; Giuliani, M.; Parrilli, E.; Branduardi, P.; Lang, C.; et al. Protein Folding and Conformational Stress in Microbial Cells Producing Recombinant Proteins: A Host Comparative Overview. *Microb. Cell Fact.* **2008**, *7*, 11.

(4) Ignatova, Z. Monitoring Protein Stability in Vivo. *Microb. Cell Fact.* **2005**, *4*, 23.

(5) Ellis, R. Macromolecular Crowding: Obvious but Underappreciated. *Trends Biochem. Sci.* **2001**, *26*, 597−604.

(6) Fulton, A. How Crowded is the Cytoplasm. *Cell* **1982**, *30*, 345−347.

(7) Zimmerman, S.; Trach, S. Estimation of Macromolecule Concentrations and Excluded Volume Effects for the Cytoplasm of Escherichia-Coli. *J. Mol. Biol.* **1991**, *222*, 599−620.

(8) Zimmerman, S.; Minton, A. Macromolecular Crowding - Biochemical, Biophysical, and Physiological Consequences. *Annu. Rev. Biophys. Biomol. Struct.* **1993**, *22*, 27−65.

(9) Hatters, D.; Minton, A.; Howlett, G. Macromolecular Crowding Accelerates Amyloid Formation by Human Apolipoprotein C-II. *J. Biol. Chem.* **2002**, *277*, 7824−7830.

(10) Uversky, V.; Cooper, E.; Bower, K.; Li, J.; Fink, A. Accelerated Alpha-Synuclein Fibrillation in Crowded Milieu. *FEBS Lett.* **2002**, *515*, 99−103.

(11) Fung, J.; Darabie, A.; McLaurin, J. Contribution of Simple Saccharides to the Stabilization of Amyloid Structure. *Biochem. Biophys. Res. Commun.* **2005**, *328*, 1067−1072.

(12) Sukenik, S.; Politi, R.; Ziserman, L.; Danino, D.; Friedler, A.; Harries, D. Crowding Alone Cannot Account for Cosolute Effect on Amyloid Aggregation. *PLoS One* **2011**, *6*, e15608.

(13) Sukenik, S.; Harries, D. Insights into the Disparate Action of Osmolytes and Macromolecular Crowders on Amyloid Formation. *Prion* **2012**, *6*, 26−31.

(14) Ellis, R.; Minton, A. Protein Aggregation in Crowded Environments. *Biol. Chem.* **2006**, *387*, 485−497.

(15) Minton, A. Models for Excluded Volume Interaction between an Unfolded Protein and Rigid Macromolecular Cosolutes: Macromolecular Crowding and Protein Stability Revisited. *Biophys. J.* **2005**, *88*, 971−985.

(16) Zhou, H.; Rivas, G.; Minton, A. P. Macromolecular Crowding and Confinement: Biochemical, Biophysical, and Potential Physiological Consequences. *Annu. Rev. Biophys.* **2008**, *37*, 375−397.

(17) Nguyen, P. H.; Li, M. S.; Stock, G.; Straub, J. E.; Thirumalai, D. Monomer Adds to Preformed Structured Oligomers of A Beta-Peptides by a Two-Stage Dock-Lock Mechanism. *Proc. Natl. Acad. Sci. U. S. A.* **2007**, *104*, 111−116.

(18) Kinjo, A.; Takada, S. Competition between Protein Folding and Aggregation with Molecular Chaperones in Crowded Solutions: Insight from Mesoscopic Simulations. *Biophys. J.* **2003**, *85*, 3521−3531.

(19) Kinjo, A. R.; Takada, S. Effects of Macromolecular Crowding on Protein Folding and Aggregation Studied by Density Functional Theory: Statics. *Phys. Rev. E* **2002**, *66*, 031911.

(20) Kinjo, A. R.; Takada, S. Effects of Macromolecular Crowding on Protein Folding and Aggregation Studied by Density Functional Theory: Dynamics. *Phys. Rev. E* **2002**, *66*, 051902.

(21) Minton, A. P. The Effect of Time-Dependent Macromolecular Crowding on the Kinetics of Protein Aggregation: A Simple Model for the Onset of Age-Related Neurodegenerative Disease. *Front. Phys.* [Online] **2014**, *2*, Article 48. DOI: 10.3389/fphy.2014.00048.

(22) O'Brien, E. P.; Straub, J. E.; Brooks, B. R.; Thirumalai, D. Influence of Nanoparticle Size and Shape on Oligomer Formation of an Amyloidogenic Peptide. *J. Phys. Chem. Lett.* **2011**, *2*, 1171−1177.

(23) Magno, A.; Caflisch, A.; Pellarin, R. Crowding Effects on Amyloid Aggregation Kinetics. *J. Phys. Chem. Lett.* **2010**, *1*, 3027−3032.

(24) Nguyen Truong Co; Hu, C.; Li, M. S. Dual Effect of Crowders on Fibrillation Kinetics of Polypeptide Chains Revealed by Lattice Models. *J. Chem. Phys.* **2013**, *138*, 185101.

(25) Cabaleiro-Lago, C.; Quinlan-Pluck, F.; Lynch, I.; Dawson, K. A.; Linse, S. Dual Effect of Amino Modified Polystyrene Nanoparticles on Amyloid Beta Protein Fibrillation. *ACS Chem. Neurosci.* **2010**, *1*, 279−287.

(26) Munishkina, L. A.; Ahmad, A.; Fink, A. L.; Uversky, V. N. Guiding Protein Aggregation with Macromolecular Crowding. *Biochemistry* **2008**, *47*, 8993−9006.

(27) Petkova, A.; Yau, W.; Tycko, R. Experimental Constraints on Quaternary Structure in Alzheimer's Beta-Amyloid Fibrils. *Biochemistry* **2006**, *45*, 498−512.

(28) Tjernberg, L.; Naslund, J.; Lindqvist, F.; Johansson, J.; Karlstrom, A.; Thyberg, J.; Terenius, L.; Nordstedt, C. Arrest of Beta-Amyloid Fibril Formation by a Pentapeptide Ligand. *J. Biol. Chem.* **1996**, *271*, 8545−8548.

(29) Balbach, J.; Ishii, Y.; Antzutkin, O.; Leapman, R.; Rizzo, N.; Dyda, F.; Reed, J.; Tycko, R. Amyloid Fibril Formation by A Beta(16−22), a Seven-Residue Fragment of the Alzheimer's Beta-Amyloid Peptide, and Structural Characterization by Solid State NMR. *Biochemistry* **2000**, *39*, 13748−13759.

(30) Zhou, H.; Rivas, G.; Minton, A. P. Macromolecular Crowding and Confinement: Biochemical, Biophysical, and Potential Physiological Consequences. *Annu. Rev. Biophys.* **2008**, *37*, 375−397.

(31) Alder, B. J.; Wainwright, T. E. Studies in Molecular Dynamics. 1. General Method. *J. Chem. Phys.* **1959**, *31*, 459−466.

(32) Wu, C.; Shea, J. Coarse-Grained Models for Protein Aggregation. *Curr. Opin. Struct. Biol.* **2011**, *21*, 209−220.

(33) Smith, A.; Hall, C. Alpha-Helix Formation: Discontinuous Molecular Dynamics on an Intermediate-Resolution Protein Model. *Proteins: Struct., Funct., Genet.* **2001**, *44*, 344−360.

(34) Nguyen, H.; Hall, C. Kinetics of Fibril Formation by Polyalanine Peptides. *J. Biol. Chem.* **2005**, *280*, 9074−9082.

(35) Marchut, A.; Hall, C. Side-Chain Interactions Determine Amyloid Formation by Model Polyglutamine Peptides in Molecular Dynamics Simulations. *Biophys. J.* **2006**, *90*, 4574−4584.

(36) Cheon, M.; Chang, I.; Hall, C. K. Extending the PRIME Model for Protein Aggregation to all 20 Amino Acids. *Proteins* **2010**, *78*, 2950−2960.

(37) Cheon, M.; Chang, I.; Hall, C. K. Spontaneous Formation of Twisted A Beta(16−22) Fibrils in Large-Scale Molecular-Dynamics Simulations. *Biophys. J.* **2011**, *101*, 2493−2501.

(38) Origin (OriginLab, N., MA) Asymmetric double sigmoidal function. http://www.originlab.com/www/helponline/origin/en/UserGuide/Asym2Sig.html.

(39) Asakura, S.; Oosawa, F. On Interaction between 2 Bodies Immersed in a Solution of Macromolecules. *J. Chem. Phys.* **1954**, *22*, 1255−1256.

(40) Cohen, S. I. A.; Vendruscolo, M.; Dobson, C. M.; Knowles, T. P. J. Nucleated Polymerization with Secondary Pathways. II. Determination of Self-Consistent Solutions to Growth Processes Described by Non-Linear Master Equations. *J. Chem. Phys.* **2011**, *135*, 065106.

(41) Cheung, M.; Klimov, D.; Thirumalai, D. Molecular Crowding Enhances Native State Stability and Refolding Rates of Globular Proteins. *Proc. Natl. Acad. Sci. U. S. A.* **2005**, *102*, 4753−4758.

(42) Asakura, S.; Oosawa, F. Interaction between Particles Suspended in Solutions of Macromolecules. *J. Polym. Sci.* **1958**, *33*, 183−192.

(43) Xue, W.; Homans, S. W.; Radford, S. E. Systematic Analysis of Nucleation-Dependent Polymerization Reveals New Insights into the Mechanism of Amyloid Self-Assembly. *Proc. Natl. Acad. Sci. U. S. A.* **2008**, *105*, 8926−8931.

(44) Lee, J.; Culyba, E. K.; Powers, E. T.; Kelly, J. W. Amyloid-Beta Forms Fibrils by Nucleated Conformational Conversion of Oligomers. *Nat. Chem. Biol.* **2011**, *7*, 602−609.

(45) Powers, E. T.; Powers, D. L. The Kinetics of Nucleated Polymerizations at High Concentrations: Amyloid Fibril Formation Near and Above the "Supercritical Concentration". *Biophys. J.* **2006**, *91*, 122−132.

(46) Kim, Y. C.; Mittal, J. Crowding Induced Entropy-Enthalpy Compensation in Protein Association Equilibria. *Phys. Rev. Lett.* **2013**, *110*, 208102.

(47) Sapir, L.; Harries, D. Origin of Enthalpic Depletion Forces. *J. Phys. Chem. Lett.* **2014**, *5*, 1061−1065.